JCTC Journal of Chemical Theory and Computation

ARTICLE

pubs.acs.org/JCTC

Development of a Polarizable Force Field for Molecular Dynamics Simulations of Poly (Ethylene Oxide) in Aqueous Solution

Oleg N. Starovoytov, Oleg Borodin, Dmitry Bedrov, and Grant D. Smith*

Department of Materials Science and Engineering, University of Utah, 122 S. Campus Drive, Salt Lake City, Utah 84112, United States

Supporting Information

ABSTRACT: We have developed a quantum chemistry-based polarizable potential for poly(ethylene oxide) (PEO) in aqueous solution based on the APPLE&P polarizable ether and the SWM4-DP polarizable water models. Ether−water interactions were parametrized to reproduce the binding energy of water with 1,2-dimethoxyethane (DME) determined from high-level quantum chemistry calculations. Simulations of DME−water and PEO−water solutions at room temperature using the new polarizable potentials yielded thermodynamic properties in good agreement with experimental results. The predicted miscibility of PEO and water as a function of the temperature was found to be strongly correlated with the predicted free energy of solvation of DME. The developed nonbonded force field parameters were found to be transferrable to poly(propylene oxide) (PPO), as confirmed by capturing, at least qualitatively, the miscibility of PPO in water as a function of the molecular weight.

I. INTRODUCTION

Poly(ethylene oxide), or PEO, also referred to as poly(ethylene glycol) or PEG, is a water-soluble polymer used in a wide variety of applications ranging from biomedical to viscosity modifications.[1−4] PEO is consolable with water for low molecular weights (less than 2000 Da) but exhibits lower critical solution temperature (LCST) behavior for higher molecular weights.[5−7] The conformations,[8−11] hydration,[12,13] hydrogen bonding,[14−17] and phase behavior[18−20] of PEO−water solutions have been the subject of extensive molecular dynamics (MD) simulations and theoretical studies, which have provided valuable insight into the behavior and properties of this important polymer solution.

The phase behavior of numerous block copolymers of water-soluble PEO and various hydrophobic polymers, including poly(propylene oxide) or PPO, in aqueous solutions has also been investigated.[1] Chemical structures of PEO and PPO as well as their shortest oligomers are shown in Figure 1. Many of these amphiphilic block copolymers utilize PEO as a soluble block and PPO as an insoluble block in diblock, triblock, or other architectures.[1−3] The well-known PEO−PPO−PEO triblock architectures as produced by BASF are referred to as Pluronics. At low concentrations and temperatures, Pluronics typically exist as fully solubilized, isolated chains or unimers. Transition from the unimer to micelle state occurs with an increase in concentration or temperature when the critical micelle concentration (CMC) or critical micelle temperature (CMT) is reached.[21] As a result, spherical micelles are formed with external PEO coronas, and central PPO cores are often observed.[22,23] Other structures are achievable with particular length ratios of hydrophilic and hydrophobic blocks.[23,24]

The self-assembly of PEO−PPO−PEO triblock polymers in water into micelles with increasing temperature is thought to be due to the increasing hydrophobicity of the central PPO block while PEO remains soluble. In this context, the phase behavior of PPO and PEO in aqueous solution is quite relevant. PPO with −OH termination groups and various molecular weights (M_w = 280−2179 Da) in water has been studied as a function of the temperature.[7,25−30] It was determined that the solubility of PPO (M_w = 400 Da) has a strong temperature dependence, being insoluble in water above ∼328 K. The position of the LCST for other molecular weight PPOs shifts to lower temperatures as the molecular weight of the polymer is increased.[26] However, PEO, while soluble with water in the temperature range of interest for applications of Pluronics micellar solutions (273−373 K), does exhibit LCST behavior at higher temperatures, as mentioned above, indicating that water becomes a poorer solvent for PEO with increasing temperature. Hence, it is likely that the changing quality of water as a solvent for both PPO and PEO with increasing temperature plays an important role in determining the phase behavior of PEO−PPO−PEO aqueous solutions.

In previous works, we have utilized atomistic molecular dynamics simulations to gain insight into the behavior of PEO in aqueous solutions.[8,12,15,17] While these studies have provided valuable insight into PEO−water solutions, including the temperature dependence of solution properties, they suffer from the shortcomings of the TIP4P water potential,[31] which was employed in these simulations. Specifically, it is well-known that the TIP4P water potential, while reproducing the density and self-diffusion coefficient of pure water at and near room temperature with reasonable accuracy,[32] does a poor job in reproducing these and other properties at high temperatures.[33] As discussed below, the temperature dependence of thermodynamic and transport properties of water can be much better reproduced utilizing water models that include atomic dipole polarizability.

In order to utilize high-quality polarizable potentials for water in simulations of PEO−water solutions, it is necessary to develop polarizable potentials for the polymers and for the polymer−water interactions. In this study, an existing, validated polarizable

Received: January 27, 2011
Published: April 29, 2011

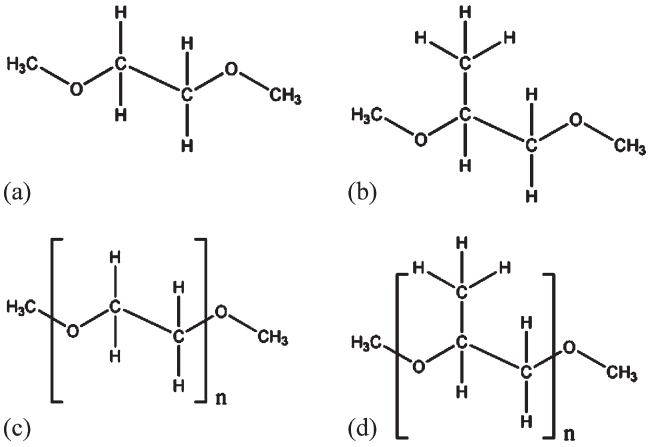

Figure 1. Chemical structures of 1,2-dimethoxyethane (a), 1,2-dimethoxypropane (b), poly(ethylene oxide) (c), and poly(propylene oxide) (d) compounds, where *n* is the number of repeat units.

potential was used for water, ethers and poly(ethers), while force field parameters for ether−water interactions were obtained on the basis of high-level quantum chemistry data. Thermodynamic and structural properties from simulations were compared with available experimental data and with simulations using our previous TIP4P-based nonpolarizable force field. We investigate the transferability of developed nonbonded force field parameters for PEO−water interactions to PPO and related ethers.

II. FORCE FIELD DEVELOPMENT

In order to develop an accurate potential for atomistic MD simulations of PEO aqueous solutions, we (a) selected an appropriate polarizable water model, (b) parametrized electrostatic interactions for the ether on the basis of quantum chemistry calculations of electrostatic potential around model PEO compounds, and (c) parametrized water−ether van der Waals interactions on the basis of a quantum chemistry study of interactions of the model ether compound with water. In the latter step, we generated two sets of nonbonded parameters as discussed below.

A. Selection of Water Model. We have considered the COS/B2[34] and COS/G2,[35] TIP4P/FQ,[36,37] POL5/TZ,[38] and SWM4-DP[39] models as candidate polarizable water models. We also show results for the nonpolarizable TIP4P[31] model for comparison. Model simplicity and accuracy in reproducing thermodynamic, dynamic, and dielectric properties were the main criteria for the selection. Specifically, the liquid density ρ, enthalpy of vaporization ΔH_{vap}, and self-diffusion coefficient D_w were considered functions of the temperature. For all models except SWM4-DP, the reported properties were obtained from the available literature.[31−41] Since the liquid state properties of water as a function of the temperature have not been reported for the SWM4-DP model, properties of interest for this model were determined by performing a series of MD simulations implementing this water model with modification of the polarization mechanism, as described in the next section. The modified water model is referred to as the SWM4-AD model, where AD stands for isotropic atomic dipole polarizability. Simulations of pure water were performed on an ensemble of 500 molecules utilizing a version of the MD simulation package Lucretius that includes isotropic atom dipole polarizability. Initially, equilibration for

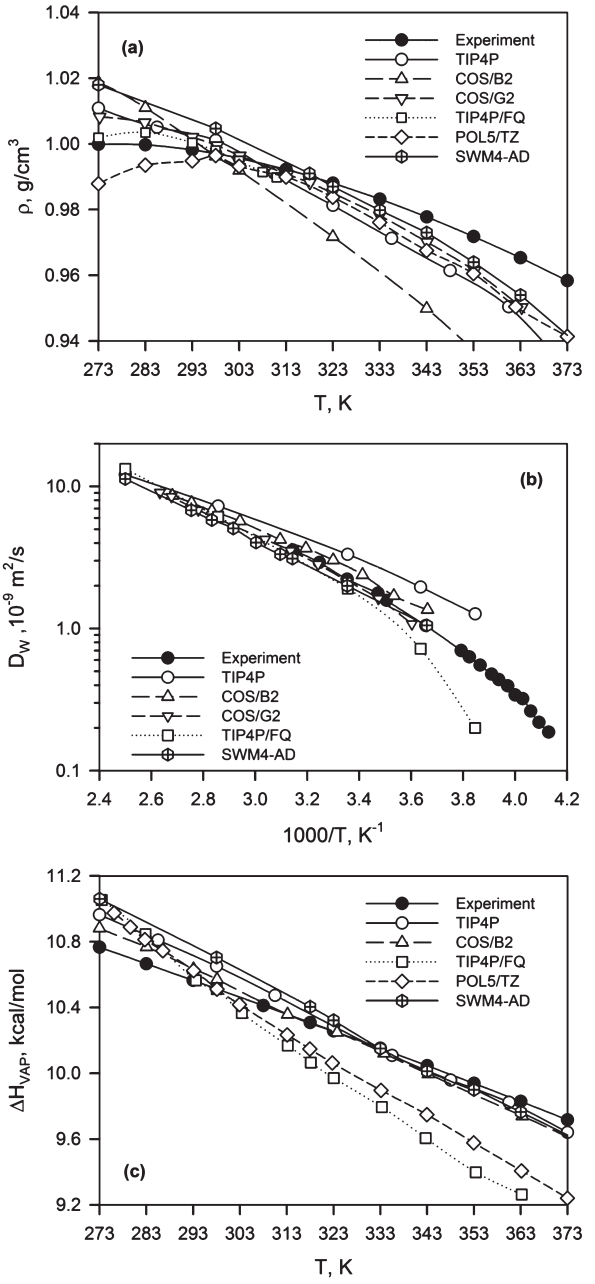

Figure 2. Water densities ρ (a), water self-diffusion coefficients D_w (b), and enthalpies of vaporization ΔH_{vap} (c) are summarized as a function of the temperature for the various models investigated. Experimental data were taken from refs 62, 80, and 91.

1 ns was performed followed by sampling trajectories of 4 ns. Isobaric−isothermal (NPT) ensemble simulations were performed at 1 atm and 298−363 K. All bond lengths were constrained during the simulation using the Shake algorithm.[42] The Ewald summation method[43] with α = 0.232 and k = 6 parameters was used to treat long-range electrostatic interactions. A multiple time step reversible propagator algorithm[44] was implemented to solve the equations of motion with a time step of 0.5 fs for valence interactions (bonds, bends, and torsions), 2 fs for nonbonded interactions within a cutoff radius of R_{cutoff} = 6.0 Å, and 4 fs for nonbonded interactions within the range of 6.0 and 10.5 Å and the reciprocal part of the electrostatic interactions.

dx.doi.org/10.1021/ct200064u |J. Chem. Theory Comput. 2011, 7, 1902–1915

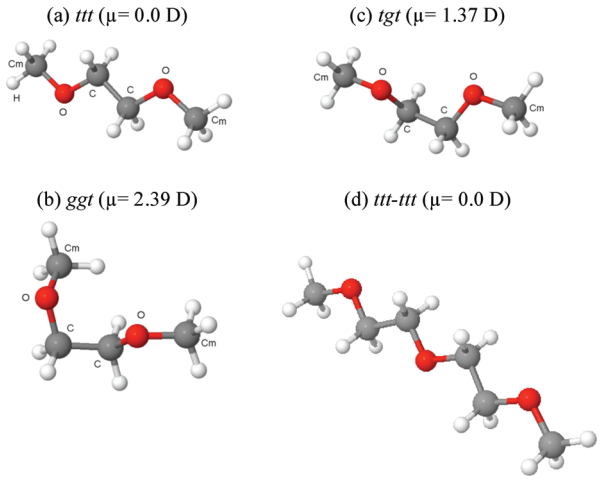

Figure 3. Hydrophilic and hydrophobic conformations of DME and diglyme are given that were used in the fitting of partial charges. Atomic labels: C_m, methoxy carbon; C, methylene carbon; and O, oxygen of ether.

Figure 2a−c show water density, enthalpy of vaporization, and the water self-diffusion coefficient as a function of the temperature for the various models investigated. Most of the water potentials do a reasonable job in reproducing experimental data at 298 K, as the potentials are typically adjusted to reproduce density at room temperature. Among the tested models, the best agreement with experiment for water density above room temperature is observed for the SWM4-AD model. The TIP4P, SWM4-AD, and COS/B2 models all reproduce experimental data for the enthalpy of vaporization reasonably well above room temperature. Therefore, these models give a reasonable estimation of the strength of intermolecular water−water interactions and its temperature dependence. All polarizable potentials were found to reproduce the water self-diffusion coefficient reasonably well while the nonpolarizable TIP4P exhibits too fast water dynamics over the entire temperature range. On the basis of these results and the fact that the SWM4-DP water model yields a dielectric constant[39,40] and surface tension[45] in good agreement with experimental results at room temperature, we have selected the SWM4-AD water model.

B. Modification of the SWM4-DP Model. The SWM4-DP polarizable water model consists of four interaction sites and Drude polarizability.[39] The latter involves a massless charge on a spring attached to the oxygen of water. In the SWM4-AD model, we have replaced Drude polarizability with an induced point dipole model. The water geometry in the SWM4-AD model was adopted unchanged from the SWM4-DP model, with an O−H bond length of 0.9572 Å and an H−O−H angle of 104.52°. The fourth (massless) site was attached to the oxygen of water by a rigid bond at a distance of 0.238 Å along the H−O−H bisector. An isotropic atomic polarizability of 1.043 $Å^3$ was assigned to the oxygen atom. Partial atomic charges were assigned to the massless particle ($-1.1074e$) and hydrogen atoms ($+0.5537e$) in accord with the original SWM4-DP model. No partial charge was allocated on the oxygen atom of water. Lennard-Jones (12−6) repulsion and dispersion parameters were taken without any adjustments (ε_{O-O} = 0.20568 kcal/mol and σ_{O-O} = 3.18030 Å). Excellent agreement was found using the SWM4-AD model with published data for the SWM4-DP model for liquid density, enthalpy of vaporization, and self-diffusion coefficient at 298 K.

Table 1. Partial Atomic Charges for DME (PEO) and DMP (PPO) (See Figure 3 for Atom Labels)

atom type	DME (PEO)	DMP (PPO)
O (C−O−C) (polymer)	0.4296	0.4068
O(C_m−O−C)	0.4348	0.4949
C_m	−0.3507	−0.4042
H_m	0.1169	0.1290
C	−0.1100	−0.2997
H	0.0576	0.0951
Lp	−0.2200	−0.2200

C. Parameterization of PEO Partial Atomic Charges. Density functional calculations were performed on 1,2-dimethoxyethane (DME) and diglyme molecules, illustrated in Figure 3, for the calculation of electrostatic potentials that were used to fit partial atomic charges. These oligomers have essentially the same local conformations as PEO in aqueous solution and similar dependence on solution composition;[8,9,46] hence, these molecules are good model compounds for PEO. The Gaussian 03 software package[47] was used for all quantum chemistry calculations. The B3LYP density functional[48−51] in combination with the aug-cc-pvDz basis set[52] was utilized on the basis of our previous studies.[12] Geometry optimization was performed for isolated DME molecule in hydrophobic *ttt* and hydrophilic *tgt* and *ggt* conformations and isolated diglyme molecule in the hydrophobic *ttt* conformation, as listed in Figure 3. Quantum chemistry calculation of the electrostatic potential for both oligomers was performed on a grid of 80 000 evenly distributed points for each single conformation. Partial atomic charges were determined using a charge fitting approach described elsewhere[53−56] that uses least-squares minimization of the objective function $\chi^2 = \sum_i^N 1/N(\phi_i^{QC} - \phi_i^{FF})^2$ relative to the electrostatic potential ϕ_i^{QC} obtained from quantum chemistry calculations. A square value of the objective function χ^2 = 1.7 was obtained. This value is much higher than the values typically obtained using such an approach (0.5−0.8). In order to improve the description of the electrostatic potentials, an additional pair of massless charges (labeled Lp) connected to ether oxygen atoms was introduced. Optimal positions and angles associated with the additional charges as well as the optimal value of the atom-based partial charges were determined simultaneously using the charge fitting approach mentioned above. The electrostatic potential ϕ_i^{FF} was calculated as a function of the angle Lp−O−Lp and distance O−Lp from the oxygen of ether. The best description of the electrostatic potential χ^2 = 0.7 was obtained for an Lp−O−Lp angle of 96°, an Lp−O separation of 0.7 Å, and an extended charge magnitude of $q_{Lp} = -0.2200e$. However, the minimum of the objective function was found to be very shallow, showing little dependence of quality of the fit in the range of ±10° for the Lp−O−Lp angle and ±0.1 for the Lp−O distance from the optimal values. Therefore, in the final version of the force field, we used an Lp−O−Lp angle of 102° and an Lp−O distance of 0.65 Å that allowed us to obtain an improved fit of DME−water binding energies (see below) and electrostatic potential around DME. The resulting assignment of partial charges for DME molecule is given in Table 1. Torsional parameters for DME/PEO were refitted to reproduce conformational energies of DME obtained from *ab initio* calculations at the MP2/aug-cc-pvDz//B3LYP/aug-cc-pvDz level. A comparison of conformational energies obtained from *ab initio* calculations and molecular mechanics calculations using PFF are given in

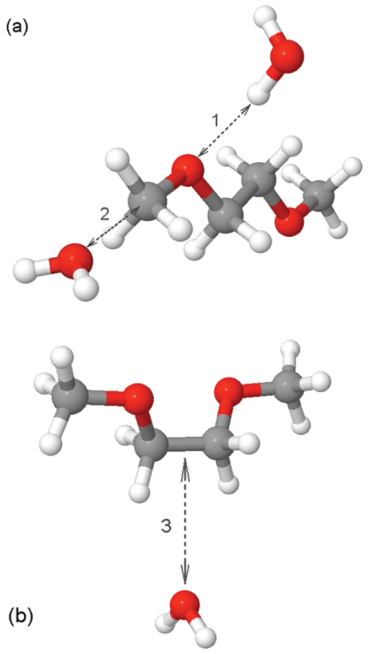

Figure 4. Schematic representations of the testing configurations are given for the calculation of DME−water binding energies in a and b, respectively. DME is in hydrophobic *ttt* (a) and hydrophilic *tgt* (b) conformations. Gray atoms represent carbons, white are hydrogens, and red are oxygen atoms. Dashed arrows indicate the directions along which the water molecule is shifted.

the Supporting Information for the most important conformers. Conformational energies predicted by PFF are in very good agreement with ab initio data and provide similar quality descriptions as our previous nonpolarizable force filed and CHARMM[57] polarizable force field.

D. Parameterization of PEO−Water Interactions. Parameters for all valence (bond, bend, and dihedral) interactions, atomic polarizabilities, and dispersion/repulsion parameters for PEO−PEO interactions were taken from the APPLE&P force field[55,58] that was found to provide a consistent description of density ρ, heat of vaporization ΔH_{vap}, and transport properties for a wide variety of liquids. The polarizable water model is described above in sections A and B, while the ether partial charges are described in section C. In order to complete our description of PEO−water systems within the atomistic polarizable force field framework, dispersion/repulsion parameters for intermolecular interactions between the ether and water need to be determined. For this purpose, extensive quantum chemistry calculations of binding energies between DME and a single water molecule were conducted. MP2/aug-cc-pvDz level calculations with basis set superposition error (BSSE) were performed using the counterpoise correction approach[59] for a number of ether−water geometries, as described below.

Water−Ether Quantum Chemistry Paths. The interactions of a water molecule with the hydrophobic *ttt* and hydrophilic *tgt* conformers of DME have been investigated along various water−ether paths designed to provide information about the interaction of water with ether oxygen atoms and methylene and methoxy groups. The paths are illustrated in Figure 4a and b. Path 1, which involves hydrogen bonding between a water hydrogen atom and an ether oxygen atom, was investigated for the DME in *ttt* conformation as well as for dimethyl ether. In the *ttt* conformer, the ether oxygen atoms of DME are on opposite sides of the molecule, facilitating investigation of hydrogen bonding between water and a single ether oxygen atom. Path 2, which involves the interaction of water with the methyl group of the methoxy group, was also investigated for the *ttt* conformer of DME. Path 3 involves the interaction of water with the "hydrophobic" side of DME, i.e., the methylene groups as opposed to the ether oxygen atoms. For all paths, initially, a locally optimized geometry was obtained at the MP2/aug-cc-pvDz level. Subsequently, the energy of the ether−water complex was determined at this level with fixed water and ether geometries, with the distance between the water oxygen being systematically increased or decreased along the water oxygen−ether oxygen vector (path 1), the water oxygen−carbon vector (paths 2), and the vector between the water oxygen and the midpoint of the carbon−carbon bond (path 3). Binding energies are reported as the difference between the BSSE (counterpoise method) corrected water−ether complex energy and that of the geometry optimized ether and water at infinite separation.

Determination of Water−Ether Dispersion/Repulsion Parameters. Dispersion/repulsion interactions between water and ether atoms were described using the Buckingham (exp-6) function for all pairs:

$$U^{\exp-6}(r_{ij}) = A_{ij}\exp(-B_{ij}r_{ij}) - \frac{C_{ij}}{r_{ij}^6} \qquad (1)$$

where i = O_w or H_w and j = C, H, O, and C_m. A_{ij} and B_{ij} are repulsion parameters, while C_{ij} is the dispersion parameter. Atom labels are shown in Figure 3. The term $D(^{12}/_{B_{ij}r_{ij}})^{12}$ is applied with $D = 5 \times 10^{-5}$ kcal/mol for all pair interactions and is essentially zero at typical nonbonded atomic separations but becomes the dominant term at $r_{ij} < 1$ Å, ensuring that $U^{\text{exp-6}}(r)$ is repulsive at distances much smaller than the size of an atom. However, this term is not applied when the A parameter is negative (see below). Dispersion C_{ij} parameters for i = O_w and j = C, H, O, and C_m were determined using the Waldman−Hagler (WH) combining rule[60] and hence were not adjustable parameters. Dispersion parameters for i = H_w and j = C, H, and C_m were set to zero with the exception of the i = H_w and j = O atomic pair, where the dispersion parameter was treated as adjustable.

The adjustable water−ether nonbonded parameters were determined by optimization of the objective function

$$\chi^2 = \sum_{\text{path}(k)} \sum_{\text{geometry}(l)} w_{kl}(\Delta U_{kl}^{\text{FF}} - \Delta U_{kl}^{\text{QC}})^2 \qquad (2)$$

where $\Delta U_{kl}^{\text{FF}}$ is the binding energy for geometry l of path k predicted by the force field, while $\Delta U_{kl}^{\text{QC}}$ is the same quantity from quantum chemistry calculations. All three DME−water binding paths (paths 1−3) were fit simultaneously. The weighting factor w_{kl} is given as

$$w_{kl} = \exp\left[-\frac{\Delta U_{kl}^{\text{QC}} - \Delta U_{kl}^{\text{EL}}}{k_b T}\right] \qquad (3)$$

where T = 298 K and $\Delta U_{kl}^{\text{EL}}$ is the electrostatic (polarization and Coulomb) contribution to the water−DME binding energy for each water−ether pair geometry, as determined from already established atomic polarizabilities and partial atomic charges. The subtraction of the electrostatic contribution to the binding energy from the total in determining the weight factor assures that each water−DME geometry is weighted in the

Table 2. Nonbonded Repulsion Parameters for Ether−Water Interactions

	PFF-1		PFF-2		PFF-1,2[a]
ether−water interaction pair	A_{ij}, kcal/mol	B_{ij}, Å^{-1}	A_{ij}, kcal/mol	B_{ij}, Å^{-1}	C_{ij}, kcal/mol Å^6
C_m-O_w	14500.76	3.28913	24893.76	3.32675	690.76
C_m-H_w	35764.40	4.85465	45764.40	4.83499	0.00
$O-O_w$	341418.22	3.94109	787505.34	4.17895	451.12
$O-H_w$[b]	−21.60				355.75
	−20.0 (PFF-3)	1.38137	1841.85	3.12997	330.0 (PFF-4)
	−16.5 (PFF-5)				310.0 (PFF-6)
$C-O_w$	29589.70	3.55272	79674.89	3.58426	665.24
$C-H_w$	34242.45	4.73729	43297.32	4.81314	0.00
$H-O_w$	11934.82	3.67285	5445.07	3.50718	138.67
$H-H_w$	2361.00	3.98266	2506.97	4.08434	0.00

[a] Dispersion parameters C_{ij} are the same for all force fields with the exception of $O-H_w$ interactions. For PFF-1,3,5, $C_{ij}(O-H_w) = 0.0$; for PFF-2,4,6, it varies as indicated in the table. [b] Only parameters for $O-H_w$ interactions were adjusted to obtain PFF-3−6. To obtain PFF-3,5, the repulsion parameter A_{ij} was the only the adjustable parameter, while to obtain PFF-4,6, the dispersion parameter C_{ij} was changed.

determination of the nonbonded parameters according to the dispersion/repulsion contribution to the binding energy of that particular geometry. In determining the molecular mechanics energy along each path, a molecular mechanics geometry optimization was first performed, and the path was determined by systematically changing the ether−water separation for the fixed ether and water geometries, analogous to the procedure used for determining the quantum chemistry paths.

The fitted force field parameters are shown in Table 2. There are two sets of fitted parameters for the water hydrogen−ether oxygen interaction. For the first, labeled PFF-1 (polarizable force field 1), the C (dispersion) parameter for the $O-H_w$ interaction, was constrained to be zero, resulting in a negative value of *A*, while in the second (PFF-2), both the *A* and *C* parameters for the $O-H_w$ interaction were treated as adjustable. Ether−water binding energies for paths 1, 2, and 3 for PFF-1 and PFF-2 as well as our previously parametrized nonpolarizable ether force field[12] (NPFF) employing the TIP4P[31] water model are compared with quantum chemistry values in Figure 5a−c. Figure 5 reveals that our PFF-1 and PFF-2 force fields provide an excellent description of the water−ether interactions and are a noticeable improvement over the NPFF. Specifically, the NPFF resulted in an underestimation of binding energies for the "hydrophilic" path 1 at separations larger than the equilibrium distance and an overestimation of binding energies of water with the methoxy carbon (path 2) and methylene carbons (path 3). These deficiencies are corrected in the PFF-1 and PFF-2 force fields.

III. MOLECULAR DYNAMICS SIMULATIONS OF ETHER-WATER SOLUTIONS

Molecular dynamics (MD) simulations of ether and poly(ether) aqueous solutions were performed in order to (1) validate the polarizable force fields by comparison of thermodynamic and transport properties with available experimental data, (2) empirically adjust PFF-1 and PFF-2 to improve agreement with experimental results, and (3) conduct initial studies of the phase behavior of PEO−water and PPO−water solutions as a function of the temperature using the newly developed polarizable potentials. Obtaining an accurate representation of PEO−water solutions as a function of the temperature was our primary motivation for the development of the polarizable force fields.

A. Simulation Methodology. MD simulations of DME, 1,2-dimethoxypropane (DMP), 12 repeat unit PEO (PEO12, with CH_3 terminal groups, 530 Da), and six repeat unit PPO (PPO6, with CH_3 terminal groups, 395 Da) in aqueous solution have been performed in the composition range (ether weight fraction) w_p = 0.01−0.93. Aqueous solutions were comprised of 1−72 solute molecules and 1200−100 water molecules depending upon the composition. The polarizable version of the Lucretius[61] simulation package was used to carry out MD simulations using a cubic simulation cell with periodic boundary conditions. The standard Shake algorithm[42] was employed to constrain the bond lengths and water geometry. Charge−charge long-range electrostatic interactions were computed employing Ewald[43] summation. The reaction field scheme[43] was implemented to handle long-range induced dipole−induced dipole calculations. The cutoff radius was 10.5 Å for nonbonded and electrostatic interactions in real space. A reversible multiple time step propagator algorithm[44] was implemented to solve the equations of motion with the parameters as specified in section A of the force field development. Simulations for T < 373 K were conducted at atmospheric pressure, while at elevated temperatures, simulations were conducted at pressures close to water saturation conditions at these temperatures to prevent potential system instability due to water evaporation. The dielectric constant ε of the solvent, which is used in reaction field calculations, was adjusted from 79 to 30 according to the experimental temperature dependence of the water dielectric constant.[62] All systems were initially equilibrated in the isothermal−isobaric ensemble until satisfactory steady state conditions (such as density of the solutions) were reached. Sampling trajectories were performed over 10 ns.

B. Free Energy of DME Solvation. The free energy of DME solvation in water, ΔG_{solv}, was determined for PFF-1 and PFF-2 using the interface transit method (IT), as described in detail in the Appendix. Briefly, a film of water comprised of 500 molecules was created in the center of an orthorhombic cell with dimensions of 24.6 Å × 24.6 Å × 84.6 Å in the *x*, *y*, and *z* directions, respectively. The water film is periodic in the *x* and *y* directions and has a thickness of approximately 29 Å in the *z* direction. The Ewald summation method[43] with α = 0.232 and k_{limit} in *x*, *y*, *z* = 6, 6, 11 was used to treat long-range electrostatic interactions. Otherwise, the simulation methodology and parameters were identical to those employed in the bulk solution simulations described above except

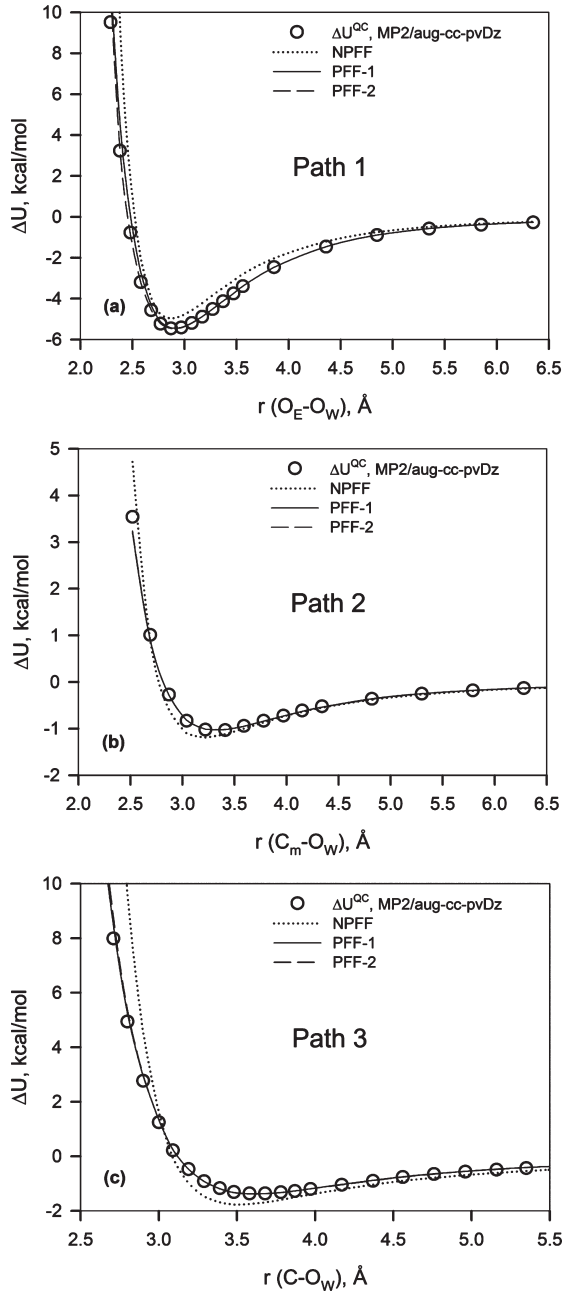

Figure 5. DME−water binding energies as obtained from quantum chemistry calculations and force field predictions for various ether−water paths.

that a single time step algorithm with a time step of 1 fs was employed instead of the multiple time step algorithm. In order to adequately thermalize the single gas-phase molecule, the solute was subjected to additional Brownian forces[63] with a friction coefficient of $\gamma = 0.002$ fs^{-1}. The average force required to constrain the center-of-mass of the DME molecule to a given Δz, $\langle F(\Delta z)\rangle$, was determined from 4 ns trajectories and 57 Δz windows ranging from 0 (in the middle of the water film) to 30 Å (middle of the vacuum phase). The free energy of transfer of the solute from the vacuum phase to the liquid phase (center of the film) is given as

$$\Delta G_{solv} = -\int_{max}^{0} \langle F(\Delta z)\rangle \, d(\Delta z) \qquad (4)$$

Table 3. Free Energy, Enthalpy, and Entropy of Solvation of DME in Aqueous Solution from MD Simulations and Experiment at 298 K[a]

FF	ΔG_{solv}, kcal/mol	ΔH_{solv}, kcal/mol	$T\Delta S$, kcal/mol
PFF-1	−5.7	−15.6	−9.9
PFF-2	−6.6	−16.8	−10.2
PFF-3	−4.9	−14.4	−9.5
PFF-4	−4.7	−14.6	−9.9
PFF-5	−3.7	−13.4	−9.7
PFF-6	−3.8	−13.5	−9.7
NPFF[b]	−5.6	−17.1	−11.5
CHARMM[c]	−3.8		
	−5.6[c]		
experiment	−4.8[d]	−14.0[e], −14.2[f]	−9.4

[a] For simulations using PFF-1 through PFF-6, the uncertainty in ΔG_{solv} is 0.6 kcal/mol and for ΔH_{solv} is 0.4 kcal/mol. [b] Nonpolarizable force field of refs 12 and 87. We note that values for the free energy and enthalpy of solvation reported in ref 87 differ from those reported here by k_BT (0.6 kcal/mol), as the previously reported values did not employ the same gas-phase and solution-phase reference states as were utilized in determining the experimental values. [c] Polarizable potential from refs 13 and 85. The values are taken from those works. [d] Ref 88. [e] Ref 89. [f] Ref 90.

Here, Δz = max corresponds to the center of the vacuum region. The direct equating of the free energy of transfer with the Gibbs free energy of solvation ΔG_{solv} is a consequence of the reference states used in defining ΔG_{solv}.[64,65] We note that although the IT method simulations are carried out in the NVE ensemble, the film is able to adjust dimensions upon insertion of the solute so as to maintain negligible normal stress in the z direction. Consequently, the free energy change determined from integration of the mean force (eq 4) is the Gibbs free energy and not the Helmholtz free energy. Validation of the IT method was carried out by testing the method to determine ΔG_{solv} for the TIP4P water model. The IT method yielded a value of $\Delta G_{solv} = -5.9 \pm 0.6$ kcal/mol, which is in excellent agreement with Monte Carlo simulation results of $\Delta G_{solv} = -6.1 \pm 0.3$ kcal/mol.[66] We also estimated the uncertainty of the free energy calculations as described in previous publications.[67,68] The IT method yields ΔG_{solv} (DME in water) = -5.7 ± 0.6 kcal/mol for PFF-1 and $\Delta G_{solv} = -6.6 \pm 0.6$ kcal/mol PFF-2, as summarized in Table 3.

C. Empirical Adjustment of the Polarizable Potentials. A comparison of ΔG_{solv} for PFF-1 and PFF-2 with experimental results (Table 3) reveals that these quantum-chemistry-fitted potentials yield water−ether interactions that are too hydrophilic. In order to improve agreement with experimental results for ΔG_{solv}, the repulsion parameter A_{O-H_w} of PFF-1 was empirically adjusted to yield force field PFF-3, and the dispersion parameter C_{O-H_w} of PFF-2 was adjusted to yield force field PFF-4. The resulting parameters are given in Table 2. All other nonbonded parameters were kept unchanged. In order to determine the new values of A_{O-H_w} and C_{O-H_w}, a thermodynamic perturbation method[69] was employed to obtain the free energy of solvation as a function of these parameters using trajectories of a single DME molecule in water using the PFF-1 and PFF-2 force fields as reference states. The resulting ΔG_{solv} values for PFF-3 and PFF-4 are in good agreement with experimental results, as shown in Table 3.

To match the experimental free energy of DME solvation, the A parameter in PFF-1 has to be reduced by about 7%

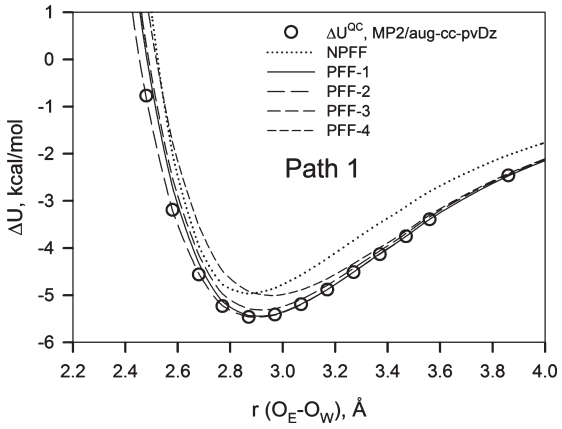

Figure 6. DME−water binding energies for path 1 as predicted by various force fields and quantum chemistry calculations.

(from −21.6 to −20.0 kcal/mol). The force field with this adjusted parameter was labeled as PFF-3. To achieve the same for PFF-2, a similar reduction by ∼7% of the dispersion parameter C_{O-H_w} was necessary (see Table 2), yielding the PFF-4 force field. To examine how these empirical adjustments of nonbonded parameters influence the description of quantum chemistry data for DME−water binding energies, we have compared the PFF-3 and PFF-4 descriptions of binding energies along paths 1−3 described above. In Figure 6, we show this comparison for the hydrophilic path 1, which shows that while description of quantum chemistry data by PFF-3 and PFF-4 is worse (compared to PFF-1 and PFF-2), it is still very good. For hydrophobic paths 2 and 3, no degradation of the description of quantum chemistry data was observed, which is expected since empirical adjustment of the O−H_w interactions should not have a significant influence on hydrophobic interactions such as interactions of water with methylene and methoxy segments of DME.

D. Enthalpy, Free Energy, and Entropy of Solvation of DME. The enthalpy of solvation of DME in water, which corresponds to the energy of the transfer of a single molecule from the gas phase to the solution at constant pressure,[64,65] was determined at 298 K and 1 atm as

$$n\Delta H_{solv}(w_{DME}) = E^{l}_{H_2O+DME}(P,T,w_{DME}) - [E^{l}_{H_2O}(P,T) - nE^{g}_{DME}(P,T)] \quad (5)$$

where the superscript l or g indicates the liquid or gas phase, E is the internal energy, and the subscripts H_2O, H_2O+DME, and DME indicate a system of 500 water molecules; a system of 500 water molecules plus n DME molecules required to yield the weight fraction of DME, W_{DME}; or a single DME molecule. We assumed that in the gas phase DME at 298 K and 1 atm behaves as an ideal gas. The internal energy of the gas phase of the DME molecule was determined from Brownian dynamics[63] simulations of 125 noninteracting DME molecules performed at 298 K. The enthalpy of solvation for DME as a function of solution composition using all four sets of nonbonded parameters (PFF-1 through PFF-4) is compared with experimental results in Table 3. The dilute solution value of ΔH_{solv} was obtained by linear extrapolation of eq 5 to infinite dilution. The entropy of solvation, calculated as $T\Delta S_{solv} = \Delta H_{solv} - \Delta G_{solv}$ is given as well.

Examination of Table 3 reveals that MD simulations using PFF-1 and PFF-2 have resulted in $\Delta H_{solv} = -15.6$ kcal/mol and $\Delta H_{solv} = -16.8$ kcal/mol, respectively, which are noticeably more than experimental values of about −14.0 kcal/mol. Interestingly, both force fields provide a basically identical description of the quantum chemistry data for paths 1−3, yet both the free energy and the enthalpy of solvation obtained using PFF-2 are about 1.0 kcal/mol more negative than for PFF-1. This difference perhaps can be attributed to different partitionings of short- and long-range nonbonded interactions between these force fields due to variation in the functional form of the O−H_w potential. Such redistribution of short- and long-range interactions, while not influencing the description of selected paths in the gas phase, clearly has a noticeable effect in the condensed phase, indicating that selection of the functional form for nonbonded interactions is important.

For the empirically adjusted (to match experimental free energy of solvation) PFF-3 and PFF-4 force fields, the enthalpy of solvation was found to be in a very good agreement with experimental results as well. Interestingly, the entropy of solvation was not affected much by empirical adjustments and, taking into account the accuracy of our calculations, is in good agreement with experimental values for all force fields (PFF-1 through PFF-4). This indicates that (a) overestimation of the free energy of DME solvation by PFF-1 and PFF-2 is primarily energetic in nature and (b) the hydration structure of DME is likely captured well by our polarizable force field and is not sensitive to variations in the functional form of nonbonded interactions.

E. Conformational Populations of DME in Water. The local conformational properties of PEO and its oligomers in water have been a subject of extensive discussions regarding key characteristics that define the unique behavior of PEO in aqueous solution. Detailed analysis and discussion of these issues can be found in our previous works. Here, we only focus on the influence of the force field on local conformations and compare predictions with available experimental data. For this purpose, we analyzed DME triad populations as a function of the composition in DME/water mixtures. In our previous simulations using NPFF, we showed that *tgt* and *tgg* conformers are hydrophilic (their population increases with increasing water content compared to the gas phase), while all other conformers, including the highly polar tg^+g^-, are hydrophobic.[8] Those results were in good agreement with previous spectroscopic studies,[70−74] with the exception of trends and populations predicted for the *tgg* and tg^+g^- conformers, which were not well resolved in the initial analysis of spectroscopic data. Subsequent to publication of our simulation results, experimental spectra were reanalyzed taking into account the potential importance of the *tgg* conformer, and the trends observed in simulations were confirmed.[75] Later, more detailed measurements and an analysis of Raman spectra were been conducted by Goutev et al.[76] to obtain triad populations of DME in water as a function of the concentration. In Figure 7a, we compare total populations of hydrophilic (*tgt* + *tgg*) and major hydrophobic (tg^+g^- + *ttt* + *ttg*) conformers, as obtained from our simulations using different force fields and Raman analysis. Data for individual triad conformers are given in the Supporting Information.

Figure 7a shows very good qualitative agreement between simulation and experimental data for all concentrations. A comparison of different force fields shows very weak dependence of conformational populations on the force field, indicating insensitivity of conformations to force field parameters varied

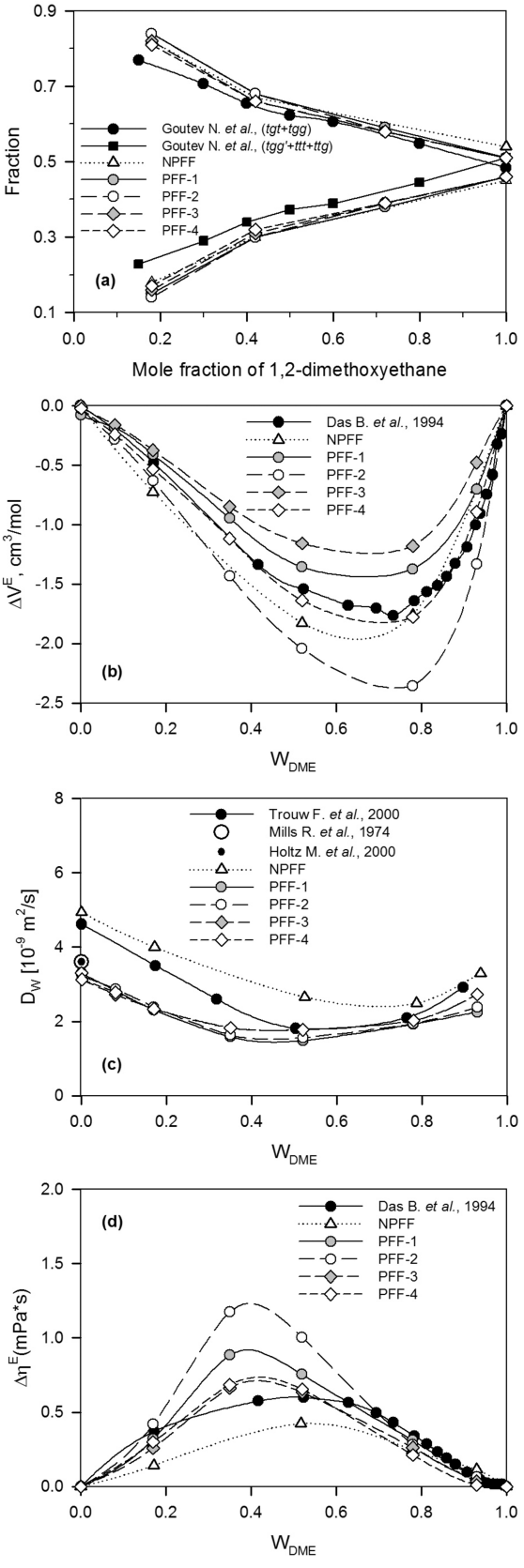

Figure 7. Comparison of conformer populations of DME in water (a), excess volume ΔV^E (b), water self-diffusion coefficient D_w (c), and excess viscosity $\Delta\eta^E$ (d) as obtained from MD simulations and experiments at 318 K for DME–water solutions. Experimental data were taken from refs 76–78, 80, and 81.

in this work despite the fact that those variations noticeably influence the free energy of solvation of DME. These observations are in agreement with our previous studies where the influence of DME conformation on solvation thermodynamics was shown to be relatively small.[10]

F. Excess Volume of DME–Water Solutions. Excess volume is often considered to be a sensitive measure of the effects of a solvation (mixing) process for two or more compounds. It can be negative or positive depending upon the strength of the solute/solvent intermolecular interactions, the difference in solute/solvent molecular sizes, and the solute/solvent solvation structures.[77] Positive excess volume usually indicates weak, unfavorable solute/solvent intermolecular interactions, while negative excess volume is an indicator of strong favorable interactions. Here, the DME–water intermolecular interactions are studied by calculating the excess volume as a function of the DME concentration. The excess molar volume ΔV^E of ether–water solutions was determined as indicated by

$$\Delta V^E = V_{\text{mixture}} - (x_{\text{solvent}} V_{\text{solvent}} + x_{\text{solute}} V_{\text{solute}}) \qquad (6)$$

where $V_{\text{mixture}} = (M_{\text{solvent}} x_{\text{solvent}} + M_{\text{solute}} x_{\text{solute}})/\rho_{\text{mixture}}$ is the molar volume of the mixture, $V_i = (M_i x_i)/\rho_i$ is the molarity of the pure components (solvent and solute), M_i is the molecular weights of the pure components, x_i is the mole fraction of the solvent or solute in the mixture, and ρ is the density. The excess molar volume for DME in 318 K aqueous solutions obtained using the four developed sets of nonbonded parameters and NPFF are compared with experimental results [77] in Figure 7b.

Examination of Figure 7b shows that simulations using PFF-1 and PFF-2 result in excess volumes in qualitative agreement with experimental results. However, simulations with PFF-1 resulted in underestimation of the excess volume, while those employing PFF-2 resulted in noticeable overestimation of the excess volume. Both force fields predict minimum weight fractions of DME between 0.6 and 0.8. A similar quality agreement for excess volume is obtained at 298 K (not shown). While for PFF-2 the more negative (than experiment) values of the excess volume are consistent with overestimation of the free energy and enthalpy of solvation, the underestimation of the excess volume by PFF-1 seems contrary to the trends observed in solvation thermodynamic properties. Despite a clear overestimation (compared to experimental results) of hydration enthalpy and free energy of solvation by PFF-1, in simulations with this force field, DME and water molecules are not able to pack efficiently enough to achieve the excess volumes observed in experimental results.

Since empirical adjustments made to PFF-1 and PFF-2 to yield PFF-3 and PFF-4 reduced the strength of DME–water interactions (as evidenced by the less favorable free energy and enthalpy of solvation as well as binding energies along path 1), it is not surprising that a significant shift to less negative values of excess volume was obtained for PFF-3 and PFF-4 force fields. While this resulted in excellent agreement between PFF-4 and experimental results, simulations using PFF-3 resulted in excess volumes in even worse agreement with experimental results than PFF-1. These data show two interesting points: (a) despite the fact that PFF-3 and PFF-4 force fields predict a similar free energy and enthalpy of solvation, the predicted excess volumes are very different, and (b) excess volume is strongly sensitive to details of O–H_w potential and, hence, the partitioning of short- and long-range nonbonded interactions. Therefore, when empirical adjustments to the force fields are made to match the free energy

(or enthalpy of solvation) of the solute, it does not necessarily guarantee accurate prediction of the excess volume.

G. Water Self-Diffusion Coefficient and Excess Viscosity in DME−Water Solutions. The self-diffusion of water is another solution property that is sensitive to the quality of the description of solute−water interactions. The mobility of water molecules near the solute can be affected by hydrogen bonding or by hydrophobic hydration. It is also well-known that water dynamics at the interface are much different from those of bulk water, including protein−water, polymer−water, and other interfaces.[78] Here, the influence of solute concentration on water dynamics is studied by obtaining the self-diffusion coefficient of water for various concentrations of DME.

The concentration dependence of the self-diffusion coefficient of water in DME−water solutions was calculated from MD simulations using PFF-1 through -4 force fields. The self-diffusion coefficient of water in DME−water solutions was determined using the Einstein relation:[43]

$$D_w = \lim_{t\to\infty} \frac{\langle (r(t) - r(0))^2 \rangle}{6t} \tag{7}$$

where $r(t)$ is the center of mass position of a molecule at time t, $\langle ... \rangle$ indicates an ensemble average, and $\langle (r(t) - r(0))^2 \rangle$ corresponds to the mean square displacement of a molecule's center of mass. Water self-diffusion coefficients were further corrected to account for the finite size effects in molecular dynamics simulations as suggested by Yeh and Hummer.[79] The viscosity η of pure SWM4-AD water was calculated at 318 K using eq 8, which is necessary for calculations of correction coefficients. The value of 0.0054P was obtained, which is in a good agreement with the experimental value of 0.0060P.[62] Corrected self-diffusion coefficients of water were 2−3% higher than initially calculated using eq 7.

The water self-diffusion coefficients obtained from MD simulations as a function of the concentration are compared with experimental results in Figure 7c. We are aware only one experimental work, by Trouw et al., using the QENS (quasi-elastic neutron scattering) technique, which reports water self-diffusion coefficients for the entire range of concentrations in DME−water solutions.[78] However, the diffusion coefficient for the pure water reported in this work is too high ($D_w = 4.6 \times 10^{-9}$ m^2 s^{-1}) compared to other experimental data obtained using the isotopic method ($D_w = 3.6 \times 10^{-9}$ m^2 s^{-1})[80] and pulsed magnetic field gradient NMR method ($D_w = 3.6 \times 10^{-9}$ m^2 s^{-1}),[81] which are also shown in Figure 7c. This mismatch might be due to the inadequacy of some assumptions of the jump diffusion model that was used to fit QENS data as discussed in ref 78. Therefore, the self-diffusion coefficient of water as a function of DME concentration reported in ref 78 is likely overestimated, particularly in dilute solutions, where it was shown that the jump diffusion model for translational motion is inconsistent with MD simulations.

Figure 7c shows that the diffusion coefficient of pure SWM4-DP water ($W_{DME} = 0$) is in good agreement with experimental results determined by isotopic and NMR methods. It is also clear that the water self-diffusion coefficient is not sensitive to variations in nonbonded parameters between polarizable force fields PFF-1 through -4 in the entire concentration range. Concentration dependences of the water self-diffusion coefficient obtained using polarizable force fields PFF-1 through -4 are in qualitative agreement with QENS data, showing a minimum weight fraction of DME at around 0.55. At higher concentrations (>0.5 DME weight fraction), simulation data are also in good quantitative agreement with QENS data. Taking into account the mismatch of experimental data in pure water, we believe that the concentration dependence of water self-diffusion using MD simulations with the polarizable force fields is quite reasonable and is certainly more accurate than previously obtained data for the nonpolarizable force field (NPFF), which are also shown in Figure 7c and noticeably overestimate water self-diffusion in the entire range of concentrations. The latter is consistent with the general trend of polarizable water models having lower diffusion coefficients compared to nonpolarizable force fields due to explicit polarization effects.[32]

Excess viscosity is another transport property useful for the validation of force field accuracy. The viscosity of DME−water solutions, pure water, and pure DME were determined using the Einstein[43] relation accounting for diagonal and nondiagonal elements as previously described.[58,82]

$$\eta = \lim_{t\to\infty} \frac{V}{20 k_B T t} \left\langle \sum (L_{\alpha\beta}(t) - L_{\alpha\beta}(0))^2 \right\rangle \tag{8}$$

where $L_{\alpha\beta}(t) = \int_0^t P_{\alpha\beta}(t')\, d(t')$, $P_{\alpha\beta}$ is the symmeterized stress tensor, $\alpha\beta$ are the components of the stress tensor, k_B is the Boltzmann constant, T is the temperature, V is the volume of the simulation cell, and $\langle ... \rangle$ indicates an ensemble average. Here, $P_{\alpha\beta}$ is the stress sensor defined a $P_{\alpha\beta} = (\sigma_{\alpha\beta} + \sigma_{\beta\alpha})/2 - (\delta_{\alpha\beta})/3 \times tr(\sigma)$, where $\sigma_{\alpha\beta}$ is a stress tensor, $\delta_{\alpha\beta} = 1$ for $\alpha = \beta$, and $\delta_{\alpha\beta} = 0$ for $\alpha \neq \beta$. The excess viscosity is given by the following relationship:

$$\Delta\eta^E = \eta_{mixture} - (x_{solvent}\eta_{solvent} + x_{solute}\eta_{solute}) \tag{9}$$

where $\Delta\eta^E$ is the excess viscosity, $\eta_{mixture}$ is the viscosity of the binary solution, η_i is the viscosity of the pure component (solvent or solute), and x_i is the molar fraction of the solvent or solute in the mixture. The excess viscosities using four sets of parameters are compared with experimental results as a function of the solution composition at 318 K in Figure 7d.

Figure 7d shows that experimental data for excess viscosity have a maximum at a weight fraction of DME of about 0.5. Simulations using PFF-1 and PFF-2 qualitatively show the same trend as experiments for excess viscosity; however, the position of the maximum appears to be shifted to a weight fraction of about 0.4, and the value at the maximum is about a factor of 2 larger than the experimental value. At dilute concentrations ($W_{DME} = 0.17$) and high concentrations ($W_{DME} > 0.7$), simulation results are in a very good agreement with experimental data. Simulations using empirically adjusted PFF-3 and PFF-4 force fields provide significantly better descriptions of the maximum value for excess viscosity, although the position of the peak is still slightly shifted to lower concentrations compared to the experimental location of the maximum. Interestingly, unlike the self-diffusion coefficient, which showed very little dependence on the version of polarizable force field, excess viscosity is much more sensitive, both to the choice of the force field (PFF-1 vs PFF-2) and to empirical adjustments of these force fields (PFF-3 and PFF-4). Finally, MD simulations using PFF-3 and PFF-4 provide a better description of excess viscosity compared to NPFF.

H. Extension of the Force Fields to Poly(Propylene Oxide)−Water Solutions. As with PEO, all bonded parameters for DMP and PPO were taken from APPLE&P.[55,58] All nonbonded

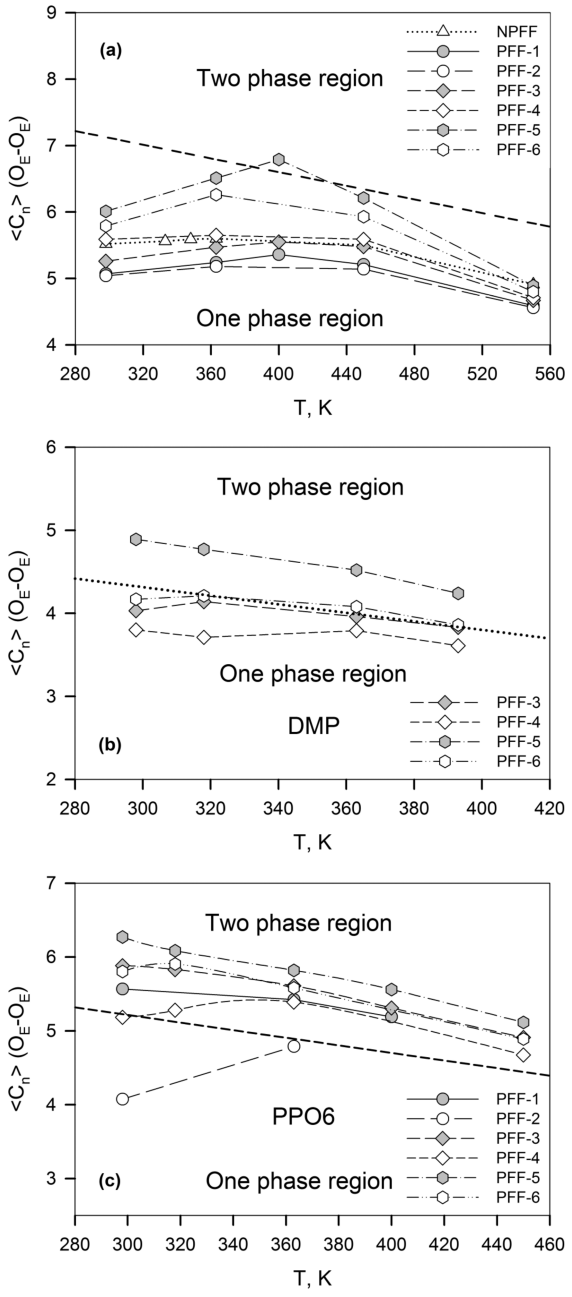

Figure 8. Ether oxygen coordination numbers and approximate phase boundaries (short double-dashed line) for PEO (a), (dotted line) for DMP (b), and (short dashed line) for PPO (c) aqueous solutions as a function of the temperature, obtained from MD simulations for various force fields investigated.

parameters for ether−water interactions were transferred as obtained for DME/PEO (see Table 2) without any additional empirical adjustments. The nonbonded parameters for the methyl−water interactions of DMP/PPO were taken as parameters for methoxy−water interactions of DME/PEO. The partial atomic charges for DMP/PPO were obtained in a similar way to that discussed in the parametrization of partial charges section, employing the most populous hydrophilic and hydrophobic conformations of DMP and 3,6-dimethyl diglyme (DMD) that could be found in a previous publication.[83] These charges are also given in Table 1.

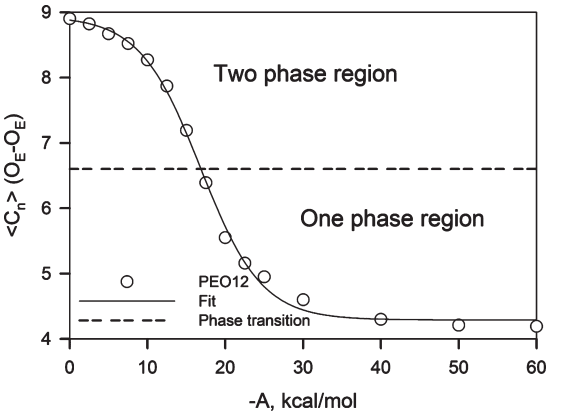

Figure 9. Ether oxygen coordination number as a function of the ether oxygen−water hydrogen intermolecular interaction parameter A at 400 K for PEO12−water solutions. Open circles indicate values obtained from MD simulations, and the solid line indicates a sigmoidal fit. The short double-dashed line indicates the approximate phase transition (inflection point).

I. Preliminary Investigation of the Phase Behavior of PEO and PPO in Aqueous Solutions. One of the goals of this work is to gain a better understanding of the correlation between the ΔG_{solv} of DME in water predicted by a force field and the predicted phase behavior of PEO and PPO in aqueous solution. For this purpose, we introduce two additional force fields, PFF-5 and PFF-6, which are variations of PFF-1,3 and PFF-2,4, respectively, with parameters given in Table 2. These force fields are more "hydrophobic" than PFF-3 and PFF-4 and have correspondingly smaller (by about 1.0 kcal/mol) ΔG_{solv} values of DME in water, as shown in Table 3.

The phase behavior of PEO−water and PPO−water was investigated as follows. Systems of 0.35 weight fractions of PEO12, DMP, and PPO6 were simulated over the temperature range of 298 to 550 K (PEO12). We used ether oxygen−ether oxygen (O_E-O_E) correlations as an order parameter to quantify the homogeneity/heterogeneity of systems. Specifically, the average O_E-O_E coordination number C_n was determined by counting the number of intra- and intermolecular O_E's within 6 Å of a given O_E. This coordination number is plotted as a function of the temperature for PEO12, DMP, and PPO6 solutions in Figure 8a−c, respectively.

PEO−Water Solutions. Figure 8a shows that initially O_E-O_E correlation increases for PEO12−water solutions with increasing temperature for all of the force fields investigated. It is reasonable to associate increased ether−ether correlation with decreasing solvent quality, which is expected for PEO−water solutions since they exhibit LCST behavior at sufficiently high molecular weights, as discussed in the Introduction. At even higher temperatures, Figure 8 reveals that ether−ether correlation decreases, consistent with the USCT behavior exhibited by PEO−water solutions. Furthermore, it can be seen that the most hydrophilic force fields (PFF-1 and PFF-2), with the largest ΔG_{solv} of DME in water, show the least ether−ether coordination, while the most hydrophobic force fields with the smallest ΔG_{solv} of DME in water (PFF-5 and PFF-6) exhibit the greatest extent of ether−ether correlation.

The relationship between the extent of O_E-O_E correlation and phase behavior is illustrated in Figure 9. Here, the O_E-O_E coordination number is plotted as a function of the "A"

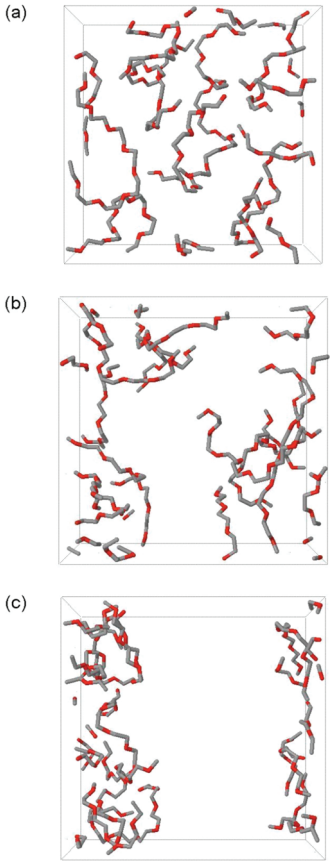

Figure 10. Snapshots for PEO12−water solutions are given as obtained from MD simulations scaling the repulsion interaction parameter *A*. Hydrogen atoms and solvent are omitted for clarity. Homogeneous solution is obtained for *A* = −30 kcal/mol (a) and *A* = −17.50 kcal/mol (b). The phase separated system is illustrated as obtained for *A* = −5 kcal/mol (c).

parameter in the O_E-H_w nonbonded energy function (eq 1) at 400 K. Here, *A* = −21.6 kcal/mol, −20.0 kcal/mol, and −16.5 kcal/mol corresponds to PFF-1, -3, and -5, respectively (see Table 2). It can be seen that ether−ether coordination increases with decreasing O_E-H_w nonbonded attraction. Also shown in Figure 10a−c are snapshots from trajectories with *A* = −30.0 kcal/mol, −17.5 kcal/mol, and −5.0 kcal/mol. Clearly *A* = −5.0 kcal/mol is phase separate, while *A* = −17.5 kcal/mol appears to be in transition and *A* = −30.0 kcal/mol corresponds to a miscible system. On the basis of this, we associate a value of $C_n(O_E-O_E) \approx 6.7$ (which corresponds to the inflection point in the $C_n(A)$ curve) with a phase separation in the 0.35 weight fraction PEO12−water solutions at this temperature. This value is temperature dependent due to thermal expansion of the system. To establish this temperature dependence, a similar $C_n(A)$ curve was obtained for 318 K, and linear extrapolation was assumed using inflection points at two temperatures to obtain the approximate phase boundary shown in Figure 8a. On the basis of theoretical predictions, PEO12 even with methyl termination is too low in molecular weight to exhibit phase separation, i.e., to exhibit LCST behavior.[20] Hence, force fields PFF-1, PFF-2, PFF-3, and PFF-4 exhibit expected behavior for the PEO12−water solutions, while PFF-5 and PFF-6 appear to be too hydrophobic in the description of ether−water interactions, as expected.

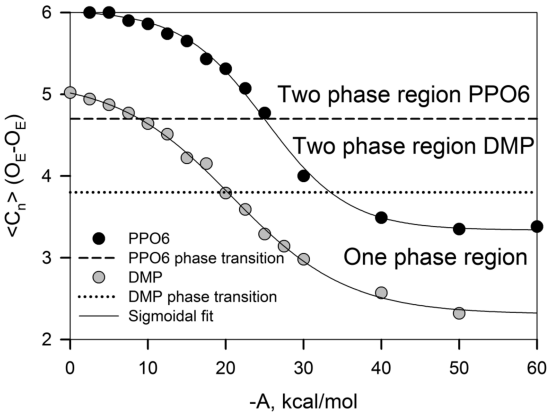

Figure 11. Ether oxygen coordination number as a function of the ether oxygen−water hydrogen intermolecular interaction parameter *A* at 400 K for DMP and PPO6. Black circles correspond to PPO6 values, and gray circles correspond to DMP values as obtained from MD simulations. Solid lines illustrate a sigmoidal fit. A short dashed line indicates the approximate phase transition for PPO6, and a dotted line indicates the approximate phase transition for DMP.

DMP−Water and PPO−Water Solutions. It has been shown experimentally that DMP is consoluble in water at least to temperatures up to 368 K.[84] We also have found experimental results for PPO−water mixtures as discussed in the Introduction. Those experimental results provide us with a position of the LCST for hydroxyl terminated PPO6 which is more hydrophilic than the methoxy terminated PPO6 simulated here. No experimental data on solvation of methoxy terminated PPO in water were found in the literature. Therefore, the position of the LCST for methoxy terminated PPO is uncertain but, on the basis of the behavior of PEO−water solutions, is likely to be significantly lower than that for hydroxyl terminated PPO. Therefore, we anticipate that 298 K is already above the LCST for PPO6−water solutions. Figure 11 shows $C_n(O_E-O_E)$ as a function of the "*A*" parameter in the O_E-H_w nonbonded potential for the 0.35 weight fraction DMP−water and PPO6−water solutions, respectively. As with PEO12−water solutions, more ether−ether clustering is observed with decreasing of the ether−water interaction strength. Similarly, the values of C_n corresponding to phase transition (inflection points) for PPO6 and DMP were obtained at two temperatures and were used to obtain approximate phase boundaries shown in Figure 8b and c. Figure 8b indicates that the DMP−water solution does not show signs of phase separation for PFF-1,2 (not shown) and PFF-4. Simulations using PFF-3 and -6 are very close or slightly above the phase boundary, while C_n obtained from simulations using PFF-5 is clearly above the phase boundary, indicating a potential phase transition for this force field. For the PPO6−water solution, where phase separation is anticipated, PFF-2 appears to provide a too hydrophilic description of ether−water interactions, while all other force fields predict phase separation at all temperatures. These results indicate that simulations using PFF-1 and -4 are the most consistent with what one can expect on the basis of existing experimental data. They predict the solubility of DMP in water yet at the same time result in phase separation for PPO6.

IV. PFF-3 VS PFF-4

Table 3 reveals that PFF-3 and PFF-4 both provide a good description of ΔG_{solv} of DME in water (as they were empirically

adjusted to do so). Furthermore, both force fields accurately describe the ΔH of solvation for DME in water. In accord with the free energy of DME solvation, PFF-3 and PFF-4 reproduce the water self-diffusion and excess viscosity of DME−water solutions at 318 K well. However, PFF-4 provides a noticeably better description of the excess volume of mixing (Figure 7b) and hence appears to be the superior force field. This is despite the fact that PFF-3 actually provides a better description of DME−water interactions along path 1, as shown in Figure 6. From these observations, we conclude that in the parametrization of polymer−water potentials

(1) parametrizing the potential to match gas phase small molecule-water interactions as obtained from high-level QC calculations is a good starting point for a potential, but empirical adjustments are likely to be required
(2) empirically adjusting the potential to reproduce the free energy of solvation of small molecules in water provides an improved description of other small molecule−water solution properties as well as polymer−water solution properties
(3) unfortunately, there is no unique way to carry out such an empirical adjustment, and variations that provide equally good descriptions of the free energy of solvation of the small molecule(s) in water can provide significantly different descriptions of other important properties
(4) point three reveals the danger of empirical adjustment of potentials to match a single solution property. The ability of the empirically adjusted potential to describe an array of solution properties should be investigated.

V. CONCLUSIONS

The ability of MD simulations to accurately reproduce the properties of PEO−water and PPO−water solutions as a function of the temperature requires a high-quality water potential and an accurate description of the interaction of ether−ether and ether−water interactions. A strong indicator of the quality of the potential is the ability of the potential to accurately describe the free energy and energy of solvation of DME in water. Our new empirically adjusted polarizable potential PFF-4 provides a good description of DME−water interactions in the gas phase as provided by high-level QC calculations while at the same time accurately reproducing the thermodynamic properties of DME−water solutions. The PFF-4 potential was found to provide a description of PEO−water, DMP−water, and PPO−water solutions consistent with experimental observations based upon preliminary simulation studies. We are currently conducting studies of higher molecular weight PEO−water solutions where LCST behavior is expected to further investigate the ability of our polarizable ether−water potential to describe PEO−water phase behavior.

The observed correlation between DME−water thermodynamic properties and the phase behavior of poly(ether)−water solutions with ΔG_{solv} for DME−water solutions provides a readily accessible method for initially evaluating the quality of an ether−water potential. For example, our previously published nonpolarizable ether−water potential[12] yields ΔG_{solv}= −5.6 kcal/mol, significantly greater than the experimental value, and hence we anticipate that this potential predicts too hydrophilic interactions between PEO and water and PPO and water. Similarly, the polarizable CHARMM potential[13] yields ΔG_{solv}= −3.8 kcal/mol (similar to our PFF-5 and PFF-6 potentials), which is apparently too hydrophobic in the description of ether−water interactions. A more recently published polarizable CHARMM potential[85] yields ΔG_{solv}= −5.6 kcal/mol, and we anticipate that this potential will yield PEO−water and PPO−water interactions that are too favorable.

APPENDIX

The interface transit method (IT) is based on the constrained force approach[86] to estimate the free energy of solvation ΔG_{solv}. In this method, a simulation cell with a film of solvent and a vacuum is set up. In order to sharpen the solvent/vacuum interface, two artificial walls parallel to the solvent/vacuum interface are applied ($x-y$ plane) on the left ZL and on the right ZR sides of the film. The biasing force from the walls $F_i^{wall}(z_i)$ acting on each atom is defined as

$$F_i^{wall}(z_i) = \begin{cases} +k(z_i - z_l)^2 & z_i < z_l \\ -k(z_i - z_r)^2 & z_i > z_r \\ 0 & z_l \le z_i \le z_r \end{cases} \quad \text{(A1)}$$

where z_i is the position of an atom i, Å; k = 5 kcal/mol·Å^2 is a force constant, and z_l and z_r are the positions for the left or right walls relative to the center of mass of the water film, Å. To ensure that the net external force (from the walls) on the film is zero at each time step, the total force from both walls was determined, and then a counter force was evenly distributed between all atoms in the film. Therefore, the effective force experienced by each atom in the film is

$$F_i^{eff}(z_i) = F_i^{wall}(z_i) - \sum_{i=1}^{N} \frac{F_i^{wall}(z_i)}{N} \quad \text{(A2)}$$

where N is the total number of atoms in the water film. As can be seen in Figure A1, application of this force sharpens the water−vacuum interface without significantly perturbing the density at the center of the film.

A single solute molecule is introduced into the system at various positions ranging from the center of the solvent film (representing a bulk-like environment) to the vacuum phase away from the film (corresponding to the ideal gas phase). The center of mass of the solute is kept at a fixed separation distance Δz from the center of mass of the film, and the force required to

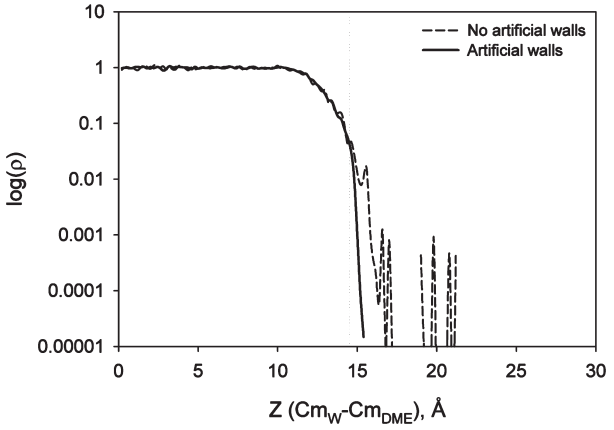

Figure A1. Water bulk distribution densities shown without constrains (no artificial walls) and with additional constraints (artificial walls applied) at the water/vacuum interface.

maintain this constraint is determined every time step and then is averaged over the entire simulation. Simulations of multiple systems with regular separation step Δz_i between the solute and center of mass of the film are conducted. In order to adequately thermalize the solute molecule in the vacuum, the solute was subjected to additional Brownian forces.

■ ASSOCIATED CONTENT

Supporting Information. Conformational energy paths for *tXt*, *gXt*, *Xtt*, and *Xgt* and populations of *tgt*, *tgg*, *tgg′*, *ttt*, and *ttg* conformers of DME as a function of the concentration at 318 K. This material is available free of charge via the Internet at http://pubs.acs.org.

■ AUTHOR INFORMATION

Corresponding Author
*E-mail: gds8@utah.edu, gsmith2@cluster2.mse.utah.edu.

■ ACKNOWLEDGMENT

We would like to acknowledge the support from the National Science Foundation through Grants CBET-0708368 and MRSEC (University of Colorado) DME-0213918.

■ REFERENCES

(1) Hamley, I. W. *The Physics of Block Copolymers*; Oxford University Press, Inc.: New York, 1998; p 295.
(2) Hadjichristiis, N.; Pispas, S.; Floudas, G. A. In *Block Copolymers: Synthetic Strategies, Physical Properties, and Applications*; Hadjichristidis, N., Ed.; John Wiley & Sons, Inc.: New York, 2003; p 290.
(3) Yallapu, M. M.; Reddy, M. K.; Labhasetwar, V. In *Biomedical Applications of Nanotechnology*; Labhasetwar, V., Leslie-Pelecky, D. L., Eds.; John Wiley & Sons, Inc.: New York, 2007; p 131.
(4) Batrakova, E. V.; Kabanov, A. V. *J. Controlled Release* **2008**, *130*, 98.
(5) Bae, Y. C.; Lambert, S. M.; Soane, D. S.; Prausnitz, J. M. *Macromolecules* **1991**, *24*, 4403.
(6) Saeki, S.; Kuwahara, N.; Nakata, M.; Kaneko, M. *Polymer* **1976**, *17*, 685.
(7) Malcolm, G. N.; Rowlinson, J. S. *J. Chem. Soc., Faraday Trans.* **1957**, *53*, 921.
(8) Bedrov, D.; Borodin, O.; Smith, G. D. *J. Phys. Chem. B* **1998**, *102*, 5683.
(9) Smith, G. D.; Bedrov, D.; Borodin, O. *J. Am. Chem. Soc.* **2000**, *122*, 9548.
(10) Smith, G. D.; Bedrov, D. *J. Phys. Chem. A* **2001**, *105*, 1283.
(11) Anderson, P. M.; Wilson, M. R. *Mol. Phys.* **2005**, *103*, 89.
(12) Smith, G. D.; Borodin, O.; Bedrov, D. *J. Comput. Chem.* **2002**, *23*, 1480.
(13) Vorobyov, I.; Anisimov, V. M.; Greene, S.; Venable, R. M.; Moser, A.; Pastor, R. W.; MacKerell, A. D. *J. Chem. Theory Comput.* **2007**, *3*, 1120.
(14) Bekiranov, S.; Bruinsma, R.; Pincus, P. *Phys. Rev. E* **1997**, *55*, 577.
(15) Smith, G. D.; Bedrov, D.; Borodin, O. *Phys. Rev. Lett.* **2000**, *85*, 5583.
(16) Dormidontova, E. E. *Macromolecules* **2002**, *35*, 987.
(17) Smith, G. D.; Bedrov, D. *Macromolecules* **2002**, *35*, 5712.
(18) Matsuyama, A.; Tanaka, F. *Phys. Rev. Lett.* **1990**, *65*, 341.
(19) Karlström, G. *J. Phys. Chem.* **1984**, *89*, 4962.
(20) Dormidontova, E. E. *Macromolecules* **2004**, *37*, 7747.
(21) Goldmints, I.; Holzwarth, J. F.; Smith, K. A.; Hatton, T. A. *Langmuir* **1997**, *13*, 6130.
(22) Goldmints, I.; vonGottberg, F. K.; Smith, K. A.; Hatton, T. A. *Langmuir* **1997**, *13*, 3659.
(23) Mortensen, K. *J. Phys. Cond. Matter* **1996**, *8*, A103.
(24) Mortensen, K.; Brown, W. *Macromolecules* **1993**, *26*, 4128.
(25) Sandell, L. S.; Goring, D. A. I. *Makromol. Chem.* **1970**, *138*, 77.
(26) Bilimova, Y. S.; Gladkovskii, G. A.; Golubev, V. M.; Medved, Z. N. *Polym. Sci. U.S.S.R* **1980**, *22*, 2456.
(27) Medved, Z. N.; Pencel, Y.; Denisova, T. A.; Lebedev, B. C. *Vysokomol. Soedin. Ser. B* **1981**, *23*, 276.
(28) Medved, Z. N.; Petrova, N. I.; Tarakanov, O. G. *Vysokomol. Soedin. Ser. B* **1982**, *24*, 674.
(29) Carlsson, M.; Hallén, D.; Linse, P. *J. Chem. Soc., Faraday Trans.* **1995**, *91*, 2081.
(30) Crowther, N. J.; Eagland, D. *J. Chem. Soc., Faraday Trans.* **1996**, *92*, 1859.
(31) Jorgensen, W. L.; Chandrasekar, J.; Madura, J. D.; Impey, R. W.; Klein, M. L. *J. Chem. Phys.* **1983**, *79*, 926.
(32) Guillot, B. *J. Mol. Liq.* **2002**, *101*, 219.
(33) Jorgensen, W. L.; Jenson, C. *J. Comput. Chem.* **1998**, *19*, 1179.
(34) Yu, H.; Hansson, T.; van Gunsteren, W. F. *J. Chem. Phys.* **2003**, *118*, 221.
(35) Yu, H.; van Gunsteren, W. F. *J. Chem. Phys.* **2004**, *121*, 9549.
(36) Rick, S. W.; Stuart, S. J.; Berne, B. J. *J. Chem. Phys.* **1994**, *101*, 6141.
(37) Rick, S. W. *J. Chem. Phys.* **2001**, *114*, 2276.
(38) Stern, H. A.; Rittner, F.; Berne, B. J.; Friesner, R. A. *J. Chem. Phys.* **2001**, *115*, 2237.
(39) Lamoureux, G.; MacKerell, A. D.; Roux, B. *J. Chem. Phys.* **2003**, *119*, 5185.
(40) Lamoureux, G.; Harder, E.; Vorobyov, I. V.; Roux, B.; MacKerell, A. D. *Chem. Phys. Lett.* **2006**, *418*, 245.
(41) English, N. J. *Mol. Phys.* **2005**, *103*, 1945.
(42) Ryckaert, J. P.; Ciccotti, G.; Berendsen, H. J. C. *J. Comput. Phys.* **1977**, *23*, 327.
(43) Allen, M. P.; Tildesley, D. J. *Computer Simulation of Liquids*; Oxford University Press: New York, 1987; p 33.
(44) Martyna, G. J.; Tuckerman, M. E.; Tobias, D. J.; Klein, M. L. *Mol. Phys.* **1996**, *87*, 1117.
(45) Ismail, A. E.; Grest, G. S.; Stevens, M. J. *J. Chem. Phys.* **2006**, *125*, 014702(1.
(46) Smith, G. D.; Bedrov, D. *Macromolecules* **2002**, *35*, 5712.
(47) Frisch, M. J., Trucks, G. W.; Schlegel, H. B.; Scuseria, G. E.; Robb, M. A.; Cheeseman, J. R.; Montgomery, J. A., Jr.; Vreven, T.; Kudin, K. N.; Burant, J. C.; Millam, J. M.; Iyengar, S. S.; Tomasi, J.; Barone, V.; Mennucci, B.; Cossi, M.; Scalmani, G.; Rega, N.; Petersson, G. A.; Nakatsuji, H.; Hada, M.; Ehara, M.; Toyota, K.; Fukuda, R.; Hasegawa, J.; Ishida, M.; Nakajima, T.; Honda, Y.; Kitao, O.; Nakai, H.; Klene, M.; Li, X.; Knox, J. E.; Hratchian, H. P.; Cross, J. B.; Bakken, V.; Adamo, C.; Jaramillo, J.; Gomperts, R.; Stratmann, R. E.; Yazyev, O.; Austin, A. J.; Cammi, R.; Pomelli, C.; Ochterski, J. W.; Ayala, P. Y.; Morokuma, K.; Voth, G. A.; Salvador, P.; Dannenberg, J. J.; Zakrzewski, V. G.; Dapprich, S.; Daniels, A. D.; Strain, M. C.; Farkas, O.; Malick, D. K.; Rabuck, A. D.; Raghavachari, K.; Foresman, J. B.; Ortiz, J. V.; Cui, Q.; Baboul, A. G.; Clifford, S.; Cioslowski, J.; Stefanov, B. B.; Liu, G.; Liashenko, A.; Piskorz, P.; Komaromi, I. M.; Fox, D. J.; Keith, T.; Al-Laham, M. A.; Peng, C. Y.; Nanayakkara, A.; Challacombe, M.; Gill, P. M. W.; Johnson, B.; Chen, W.; Wong, M. W.; Gonzalez, C.; Pople, J. A. *Gaussian 03*, Revision E.01; Gaussian, Inc.: Wallingford, CT, 2004.
(48) Lee, C.; Yang, W.; Parr, R. G. *Phys. Rev. B* **1988**, *37*, 785.
(49) Becke, A. D. *Phys. Rev. A* **1988**, *38*, 3098.
(50) Becke, A. D. *J. Chem. Phys.* **1992**, *98*, 1372.
(51) Becke, A. D. *J. Chem. Phys.* **1992**, *98*, 5648.
(52) Kendall, R. A.; Dunning, T. H. *J. Chem. Phys.* **1992**, *96*, 6796.
(53) Borodin, O.; Smith, G. D. *J. Phys. Chem. B* **2003**, *107*, 6801.
(54) Smith, G. D.; Borodin, O. In *Molecular Simulation Methods for Predicting Polymer Properties*; Galiatsatos, V.; Ed.; John Wiley & Sons Inc: New York, 2005; p 47.
(55) Borodin, O.; Smith, G. D. *J. Phys. Chem. B* **2006**, *110*, 6279.

(56) Borodin, O.; Smith, G. D. *J. Phys. Chem. B* **2009**, *113*, 1763.
(57) Lee, H.; Venable, R. M.; MacKerell, A. D.; Pastor, R. W. *Biophys. J.* **2008**, *95*, 1590.
(58) Borodin, O. *J. Phys. Chem. B* **2009**, *113*, 11463.
(59) Boys, S. F.; Bernardi, F. *Mol. Phys.* **1970**, *19*, 553.
(60) Waldman, M.; Hagler, A. T. *J. Comput. Chem.* **1993**, *14*, 1077.
(61) http://www.eng.utah.edu/~gdsmith/lucretius.html (accessed April 2011).
(62) *CRC Handbook of Chemistry and Physics*; Lide, D. R., Ed.; CRC Press: Boca Raton, FL, 2006.
(63) Gunsteren, W. F.; Berendsen, H. J. C. *Mol. Phys.* **1982**, *45*, 637.
(64) Ben-Naim, A.; Marcus, Y. *J. Chem. Phys.* **1984**, *81*, 2016.
(65) Ben-Naim, A. *Statistical Thermodynamics for Chemists and Biochemists*; Plenum Press: New York, 1992; p 459.
(66) Jorgensen, W. L.; Blake, J. F.; Buckner, J. K. *Chem. Phys.* **1989**, *129*, 193.
(67) Li, L. W.; Davande, H.; Bedrov, D.; Smith, G. D. *J. Phys. Chem. B* **2007**, *111*, 4067.
(68) Bedrov, D.; Smith, G. D.; Davande, H.; Li, L. W. *J. Phys. Chem. B* **2008**, *112*, 2078.
(69) Simkin, B. Y.; Sheikhet, I. I. In *Quantum Chemical and Statistical Theory of Solutions: A Computational Approach*; Kemp, T. J., Ed.; Ellis Horwood Limited: New York, 1995; p 155.
(70) Yoshida, H.; Takikawa, K.; Kaneko, I.; Matsuura, H. *J. Mol. Struct.* **1993**, *311*, 205.
(71) Matsuura, H.; Sagawa, T. *J. Mol. Liq.* **1995**, *65/66*, 313.
(72) Masatoki, S.; Takamura, M.; Matsuura, H.; Kamogawa, K.; Kitagawa, T. *Chem. Lett.* **1995**, 991.
(73) Yoshida, H.; Tanaka, T.; Matsuura, H. *Chem. Lett.* **1996**, 637.
(74) Begum, R.; Matsuura, H. *J. Chem. Soc., Faraday Trans.* **1997**, *93*, 3839.
(75) Yoshida, H.; Matsuura, H. *J. Phys. Chem. A* **1998**, *102*, 2691.
(76) Goutev, N.; Ohno, K.; Matsuura, H. *J. Phys. Chem. A* **2000**, *104*, 9226.
(77) Das, B.; Roy, M. N.; Hazra, D. K. *Indian J. Chem. Technol.* **1994**, *1*, 93.
(78) Trouw, F.; Bedrov, D.; Borodin, O.; Smith, G. D. *J. Chem. Phys.* **2000**, 01.
(79) Yeh, I.-C.; Hummer, G. *J. Phys. Chem. B* **2004**, *108*, 15873.
(80) Mills, R. *Mol. Motions Liq.* **1974**, 391.
(81) Holtz, M.; Heil, S. R.; Sacco, A. *Phys. Chem. Chem. Phys.* **2000**, *2*, 4740.
(82) Daivis, P. J.; Evans, D. J. *J. Chem. Phys.* **1994**, *100*, 541.
(83) Smith, G. D.; Borodin, O.; Bedrov, D. *J. Phys. Chem. A* **1998**, *102*, 10318.
(84) Stephenson, R. M. *J. Chem. Eng. Data* **1993**, *38*, 134.
(85) Baker, C. M.; MacKerell, A. D. *J. Mol. Model.* **2009**, *16*, 567.
(86) Mülders, T.; Krüger, P.; Swegat, W.; Schlitter, J. *J. Chem. Phys.* **1996**, *104*, 4869.
(87) Smith, G. D.; Bedrov, D. *J. Phys. Chem. B* **2003**, *107*, 3095.
(88) Cabani, S.; Mollica, V. *J. Chem. Soc., Faraday Trans.* **1978**, *74*, 2667.
(89) Dohnal, V.; Roux, A. H.; Hynek, V. *J. Solution Chem.* **1994**, *23*, 889.
(90) Kustov, A. V.; Antonova, O. A.; Korolev, V. P. *J. Solution Chem.* **2002**, *31*, 671.
(91) Gillen, K. T.; Douglass, D. C.; Hoch, M. J. R. *J. Chem. Phys.* **1972**, *57*, 5117.